ACS APPLIED MATERIALS & INTERFACES

Research Article

www.acsami.org

Decorating CdTe QD-Embedded Mesoporous Silica Nanospheres with Ag NPs to Prevent Bacteria Invasion for Enhanced Anticounterfeit Applications

Yangyang Gao,[†,‡] Qigeqi Dong,[†,§] Shi Lan,[⊥] Qian Cai,[‡] Oudjaniyobi Simalou,[∥] Shiqi Zhang,[#] Ge Gao,[△] Harnoode Chokto,[‡] and Alideertu Dong*[,‡]

[‡]College of Chemistry and Chemical Engineering and [§]College of Life Science, Inner Mongolia University, Hohhot 010021, People's Republic of China

[⊥]College of Science, Inner Mongolia Agricultural University, Hohhot 010018, People's Republic of China

[∥]Département de Chimie, Faculté Des Sciences (FDS), Université de Lomé (UL), BP 1515 Lome, Togo

[#]PhD School of Materiaux, Mechanics, Environnement, Energy, Process and Production Engineering (I-MEP2), University of Grenoble, Grenoble 38031, France

[△]College of Chemistry, Jilin University, Changchun 130021, People's Republic of China

Supporting Information

ABSTRACT: Quantum dots (QDs) as potent candidates possess advantageous superiority in fluorescence imaging applications, but they are susceptible to the biological circumstances (e.g., bacterial environment), leading to fluorescence quenching or lose of fluorescent properties. In this work, CdTe QDs were embedded into mesoporous silica nanospheres (m-SiO_2 NSs) for preventing QD agglomeration, and then CdTe QD-embedded m-SiO_2 NSs (m-SiO_2/CdTe NSs) were modified with Ag nanoparticles (Ag NPs) to prevent bacteria invasion for enhanced anticounterfeit applications. The m-SiO_2 NSs, which serve as intermediate layers to combine CdTe QDs with Ag NPs, help us establish a highly fluorescent and long-term antibacterial system (i.e., m-SiO_2/CdTe/Ag NSs). More importantly, CdTe QD-embedded m-SiO_2 NSs showed fluorescence quenching when they encounter bacteria, which was avoided by attaching Ag NPs outside. Ag NPs are superior to CdTe QDs for preventing bacteria invasion because of the structure (well-dispersed Ag NPs), size (small diameter), and surface charge (positive zeta potentials) of Ag NPs. The plausible antibacterial mechanisms of m-SiO_2/CdTe/Ag NSs toward both Gram-positive and Gram-negative bacteria were established. As for potential applications, m-SiO_2/CdTe/Ag NSs were developed as fluorescent anticounterfeiting ink for enhanced imaging applications.

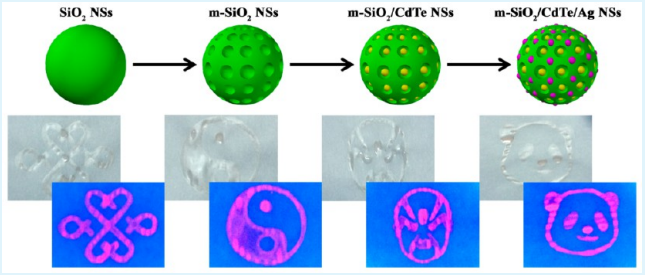

KEYWORDS: *mesoporous SiO_2, CdTe QDs, fluorescent, Ag NPs, antibacterial, anticounterfeit*

INTRODUCTION

Quantum dots (QDs) as new fluorophores have provoked increasing intensive research interests in the past few decades.[1] QDs have been distinguished from traditional fluorescent materials for their various potential applications.[2] Unlike the organic dyes, QDs can endow outstanding merits, e.g., broad absorption/narrow emission, high fluorescence efficiency, large effective Stokes shift, long fluorescence lifetime, composition/size tunability, and high stability to lights and chemicals.[3] These merits underline their superiority in fields of fluorescence imaging, for example, fluorescent anticounterfeiting applications. Despite amazing advances in the development of QDs, there remains broad research space for this nascent topic. In particular, the practical applications of QDs have to overcome their vulnerability in the biological environment.[4] Exploring alternative routes to widen their applications are still highly required. Surface modification is deemed to be a trustworthy technique for their practical applications.[5] One key promising approach is incorporating QDs in porous silica matrix, which provide them better physical and chemical stability.[6] Porous silica is considered to be one of the most potent porous structures as it generally possesses good biocompatibility and ease of surface modification that provides reservoirs for loading various functional molecules and active sites for linking other targeted molecules by covalent association.[7] Therefore, QD-embedded porous silica may not only prevent QD agglomeration but also offer the quantum confinement effect to take advantage of the superior properties of both QDs and porous silica.[8] Despite exciting improvement achieved from porous silica, the embedded QDs are still susceptible to the biological

Received: March 20, 2015
Accepted: April 22, 2015
Published: April 22, 2015

DOI: 10.1021/acsami.5b02472
ACS Appl. Mater. Interfaces 2015, 7, 10022−10033

Scheme 1. Formation Schematics of m-SiO_2/CdTe/Ag NSs

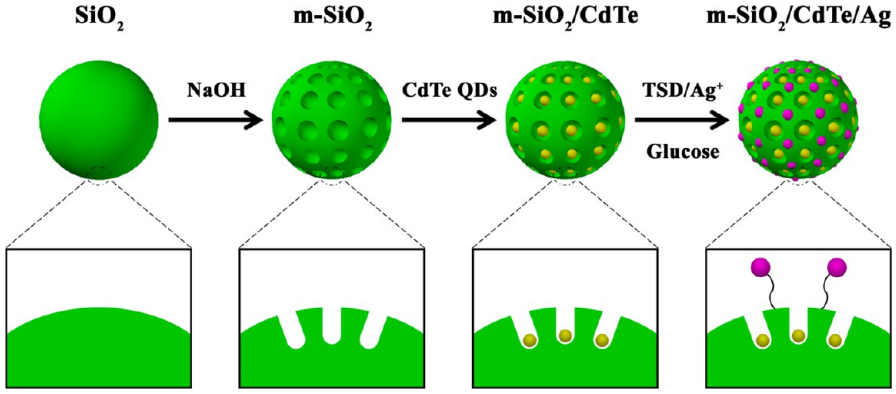

environment and easily lose their fluorescence because of their biological activity.[9] In particular, bacterial invasion can pose a serious threat to stability of the QDs.[9]

Recent studies implied that silver nanoparticles (Ag NPs) draw interest for their unique and powerful antibacterial capabilities against a wide spectrum of bacteria.[10] Ag NPs have been widely employed to prevent bacterial infection for medical purposes.[11] It was acknowledged that the biocidal materials constituting Ag NPs are more popular compared with other metallic nanoparticles.[12] Nevertheless, practical applications of Ag NPs are often hampered by oxidization reactions, which may cause aggregation and even loss of antibacterial activity.[13] In response to these problems, inorganic carriers, e.g., porous silica, have been developed as Ag NPs carrying antibacterial agents.[14] One effective strategy for loading Ag NPs is to deposit them on the surface of porous silica by chemical binding method.[15] Because Ag NPs containing silica agents are easily achieved, they are predicted to be more potential candidates than conventional Ag NPs.[16] Porous silica matrix can protect Ag NPs from aggregation, and the products can release Ag ions slowly and continuously to realize long-term antibacterial activity.[17]

Herein, we focus on a simple approach to immobilize Ag NPs onto CdTe QDs embedded mesoporous silica nanospheres (m-SiO_2 NSs) by a three-step process for enhanced anticounterfeit application (Scheme 1). Using m-SiO_2 NSs as intermediate layers to combine CdTe QDs with Ag NPs can help us construct fluorescent anticounterfeiting candidates with long-term antibacterial capabilities. Moreover, the intermediate m-SiO_2 NSs might not only solve the problems of lattice mismatch and chemical dissimilarity between these two components but also somehow protect CdTe QDs from fluorescence quenching by Ag NPs. Given that Ag NPs can prevent CdTe QDs from bacterial invasion, we believe that this approach could offer a potential possibility for developing enhanced fluorescent anticounterfeiting systems such as security of tickets, certificates, money, checks, bank notes, trademarks, invoices, etc.

EXPERIMENTAL SECTION

Materials. All the chemicals used in this work were of analytical grade and were used without further purification. Tetraethyl orthosilicate (TEOS) was obtained from Tianjin Guangfu Fine Chemical Research Institute. Anhydrous ethanol, ammonium hydroxide (25 wt % NH_3 in water), and sodium hydroxide (NaOH, 96.0%) were purchased from Beijing Chemical Company. Cadmium chloride ($CdCl_2$, 99%), 3-mercaptopropionic acid (MPA, $C_3H_6O_2S$, 99%), and sodium tellurite (Na_2TeO_3, 97%) were available from Aladdin Reagent Company. Sodium borohydride ($NaBH_4$), silver nitrate ($AgNO_3$), and glucose were provided by Sinopharm Chemical Reagent Co. Ltd.

Synthesis of m-SiO_2/CdTe/Ag NSs. The synthesis of m-SiO_2/CdTe/Ag NSs was accomplished via a three-step process. In a typical procedure, about 1.0 g of SiO_2 NSs (prepared from the stöber method as shown in the Supporting Information) were dispersed in 100 mL of water followed by addition of 4.0 mL of NaOH solution (0.1 g/mL). The mixture was vigorously stirred in a closed flask for 12 h to obtain m-SiO_2 NSs. About 0.5 g of m-SiO_2 NSs was dispersed in 50 mL of water followed by addition of 2.0 mL of MPA-capped CdTe QD solution (0.1 g/mL, synthetic procedure is shown in Supporting Information). The mixture solution was mechanically stirred at room temperature for 6 h to embed CdTe QDs into m-SiO_2 NSs. About 0.2 g of m-SiO_2/CdTe NSs was mixed with 30 μL of TSD and 25 mL of ethanol, and the mixture was mechanically stirred at 40 °C for 12 h. About 0.1 g of TSD-modified m-SiO_2/CdTe NSs was dispersed in 50 mL of $AgNO_3$ solution (0.1 mol/L), which was stirred by a mechanical stirrer at room temperature for 1 h, and then 50 mL of glucose solution (0.1 g/mL) was added into the mixture solution with 1 h stirring. The as-synthesized m-SiO_2/CdTe/Ag NSs was centrifuged, water-washed three times, and dried under vacuum.

Characterizations. Morphology, microstructure, and size distribution were examined by scanning electron microscopy (SEM, Shimadzu SSX-550), high resolution transmission electron microscopy (HRTEM, JEM-200CX), and transmission electron microscopy (TEM, JEM-200CX). The energy-dispersive X-ray (EDX) was performed during the scanning electron microscope measurements. The zeta potentials were measured using a multifunctional zeta PALS potential and particle size analyzer (Brookhaven Instruments Corporation). The XRD patterns were obtained with a Siemens model D5000 diffractometer equipped with a copper anode producing X-rays with a wavelength of 1.5418 Å. FTIR spectra were recorded by using a Thermo Nicolet (Woburn, MA) Avatar 370 FTIR spectrometer. A nitrogen adsorption instrument (Micrometritics ASAP2020) was applied to study the Brunauer–Emmett–Teller (BET) surface area and the porosity. UV–visible absorption spectra were collected with a Hitachi U-3900H spectrophotometer over the wavelength range from 300 to 700 nm. The amount of silver and cadmium were determined using a PerkinElmer optima 2100 Inductively Coupled Plasma-Optical Emission (ICP-OES) spectrometer. The fluorescence microscopy images were taken by an Olympus IX-71 and Nuance multispectral imaging system (Cambridge Research & Instrumentation, Inc.). The fluorescence spectra were recorded using a Hitachi F-4500 fluorescence spectrophotometer.

Bacterial Growth Conditions. As for antibacterial test, *Staphylococcus aureus* (*S. aureus*, ATCC 25923, Gram-positive) and *Escherichia coli* (*E. coli*, ATCC 25922, Gram-negative) were used as model microorganisms. Bacteria were grown overnight at 37 °C under agitation (200 rpm) in Luria–Bertani (LB) growth medium. Bacterial cells were harvested by centrifugation, washed twice with phosphate-buffered saline (PBS, pH 7.4), and diluted to concentrations of 1 tme 10^6 colony-forming units/mL (CFU/mL).

DOI: 10.1021/acsami.5b02472
ACS Appl. Mater. Interfaces 2015, 7, 10022–10033

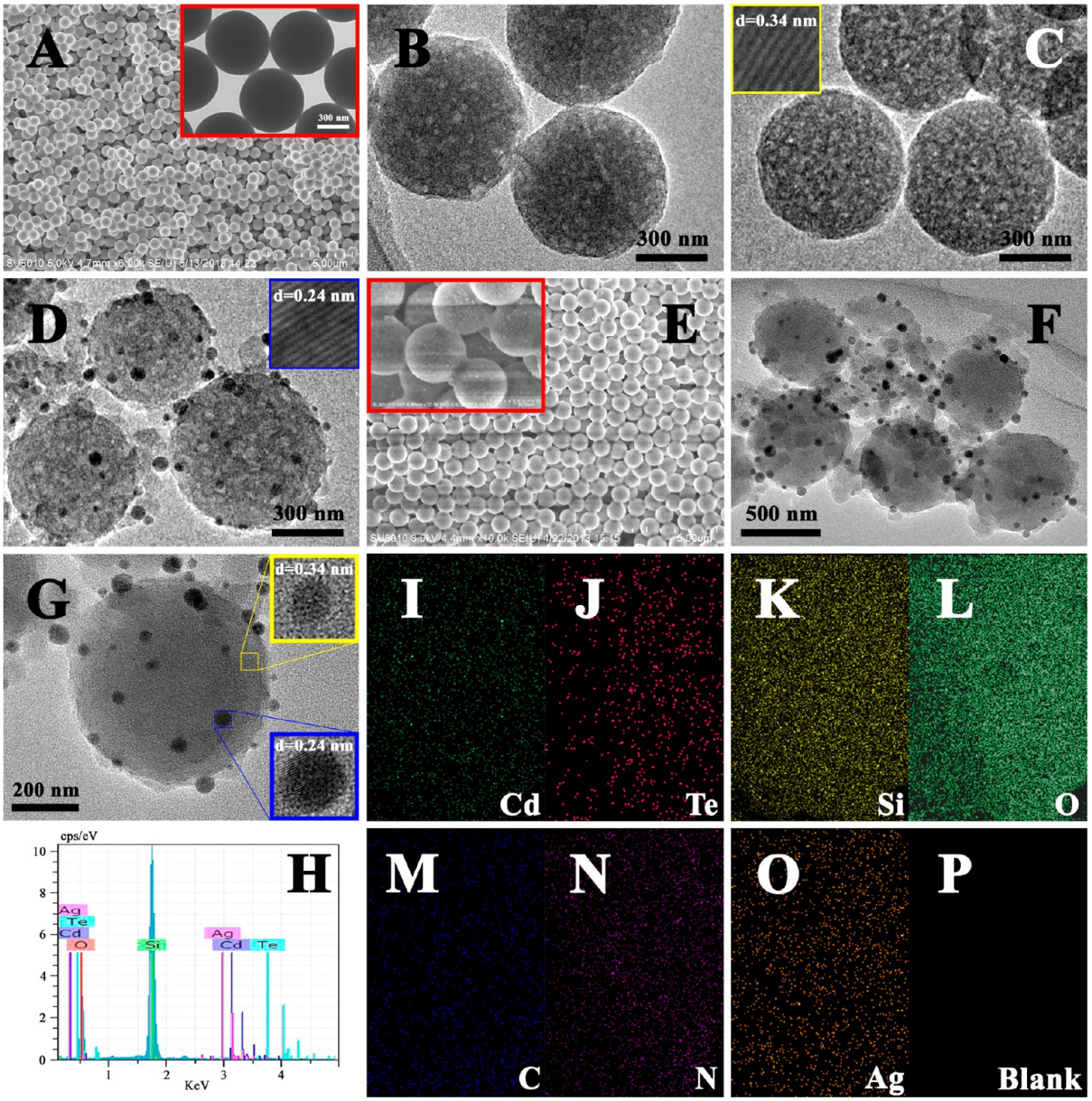

Figure 1. (A) SEM and TEM (inset) of solid SiO_2 NSs; (B) TEM of m-SiO_2 NSs; (C) TEM and HRTEM (insert) of m-SiO_2/CdTe NSs; (D) TEM and HRTEM (insert) of m-SiO_2/Ag NSs; (E) SEM and high-magnification image of m-SiO_2/CdTe/Ag NSs; (F, G) TEM and HRTEM (inset in G) of m-SiO_2/CdTe/Ag NSs; (H) EDX pattern of m-SiO_2/CdTe/Ag NSs; (I–P) elemental mapping of m-SiO_2/CdTe/Ag NSs.

Plate Counting Method. Antibacterial activities of m-SiO_2/CdTe/Ag NSs were evaluated in LB agar culture plate via the plate counting method.[18] The m-SiO_2/CdTe/Ag NSs (5.0 mg) was dispersed in 450 μL of sterilized distilled water and vortexed for 10 min. Subsequently,a bacteria suspension (50 μL, 1 × 10^6 CFU/mL) was added into the above-mentioned m-SiO_2/CdTe/Ag NSs suspension (450 μL), mixed well, and incubated under constant shaking. The resulting mixture was serially diluted, and then 100 μL of each dilution was dispersed onto LB agar plates. Bacterial colonies on the cultural plates were counted after incubation at 37 °C for 24 h. The m-SiO_2 NSs, CdTe QDs, Ag NPs, m-SiO_2/CdTe NSs, and m-SiO_2/Ag NSs were used as comparative controls. Time kill assay of m-SiO_2/CdTe/Ag NSs was performed using plate counting method.

Inhibition Zone Study. The antibacterial activities of m-SiO_2/CdTe/Ag NSs were also tested by the inhibition zone study using a modified Kirby-Bauer technique.[19] The m-SiO_2/CdTe/Ag NSs powder (0.3 g) was grinded well and added into a circular mold with a diameter of 1.0 cm, and then pressed at room temperature using a tablet machine to obtain the sample disc. The surface of LB agar plate and tryptic soy agar plate was overlaid with *E. coli* (500 μL, 10^6 CFU/mL) and *S. aureus* (500 μL, 1 × 10^6 CFU/mL), respectively. The plates were then allowed to stand at 37 °C. Then the above-mentioned sample disc was placed onto the surface of the bacteria-containing agar plate. After incubation (37 °C, 24 h), the inhibition zone around the product was recorded. The m-SiO_2/CdTe NSs and m-SiO_2/Ag NSs were used as well as comparative controls.

RESULTS AND DISCUSSION

In this work, we detailed a simple synthetic route to produce fluorescent/antibacterial bifunctional m-SiO_2/CdTe/Ag NSs. The overall synthetic procedure of m-SiO_2/CdTe/Ag NSs is illustrated in Scheme 1. Solid SiO_2 NSs formed via the stöber process based on the hydrolysis of tetraethyl orthosilicate (TEOS).[20] Using the etching method, the mesoporous silica (m-SiO_2) NSs with mesopores on their wall were obtained. Introducing m-SiO_2 NSs as templates not only achieves the

DOI: 10.1021/acsami.5b02472
ACS Appl. Mater. Interfaces 2015, 7, 10022–10033

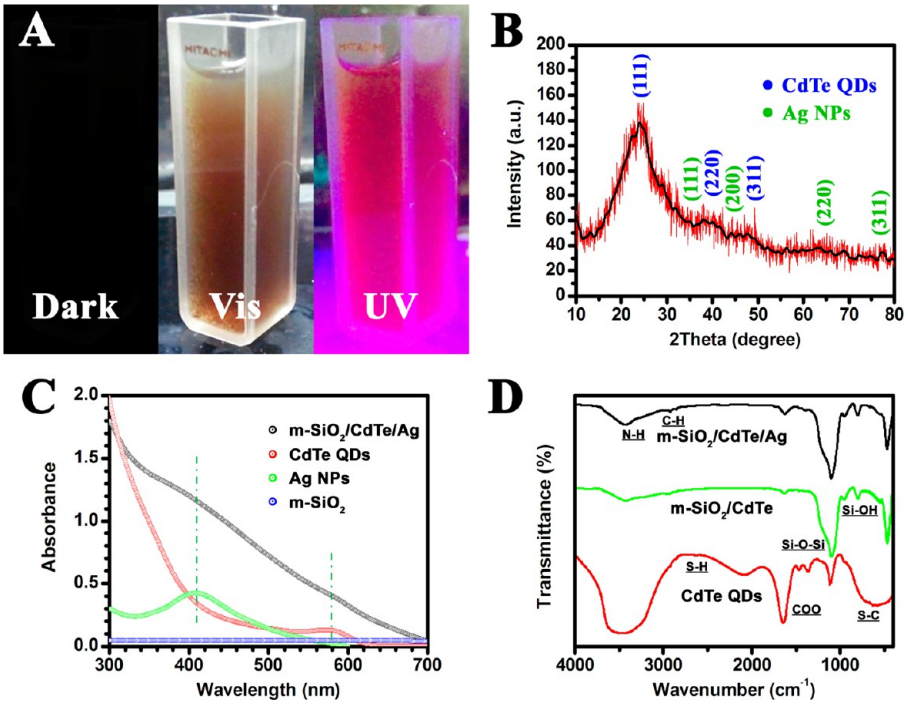

Figure 2. (A) Photos of m-SiO_2/CdTe/Ag NSs solution under dark, visible light, and λ = 365 nm UV beam; (B) XRD pattern of m-SiO_2/CdTe/Ag NSs; (C) UV−vis spectrum of m-SiO_2 NSs, CdTe QDs, Ag NPs, and m-SiO_2/CdTe/Ag NSs; (D) FTIR spectrum of CdTe QDs, m-SiO_2/CdTe NSs, and m-SiO_2/CdTe/Ag NSs.

target of enlarging the activated surface area but also realizes the immobilization of CdTe QDs. 3-Mercaptopropionic acid (MPA) stabilized CdTe QDs (MPA-CdTe QDs) trapped into the mesopores by the aid of mechanical stirring to obtain m-SiO_2/CdTe NSs. To attach Ag NPs, the surface of m-SiO_2/CdTe NSs was then modified with N-(amino-ethyl)-amino-propyl trimethoxysilane (TSD, siliane coupling agent), which can offer strong chemical binding between m-SiO_2/CdTe NSs and Ag NPs. TSD can prevent CdTe QDs leaching out from mesopores or/and aggregating on the surfaces. More importantly, TSD can also serve as the isolating agent, which can avoid fluorescence quenching induced by the direct contacting CdTe QDs with Ag NPs. Silver ions (Ag^+) can be easily attached onto TSD decorated m-SiO_2/CdTe NSs, and then reduced to Ag seeds by the well-known silver-mirror reaction to obtain the target m-SiO_2/CdTe/Ag NSs.[21] The synergism between CdTe QDs and Ag NPs can prevent fluorescent materials from microbial threats, which can enhance their anticounterfeit applications.

The evidence for the confirmation of products were inferred from different techniques. TEM image (Figure 1A) shows that solid SiO_2 NSs have monodisperse spherical shapes with an average size of 616.44 nm, which are further confirmed by the inset TEM in Figure 1A and Figure S1 in Supporting Information. Most importantly, the surface of SiO_2 NSs is quite smooth without any flaws. Upon NaOH etching, some solid silica matrix on surfaces being converted to soluble silicate oligomers, and network of the silica particle become porous.[22] TEM images of m-SiO_2 NSs in Figure 1B and Figure S2 in the Supporting Information show rough appearance with small holes and gaps on the surface of the etched particles. The average diameter decreases to 608.01 nm, whereas the original spherical shape is still retained (Figure S2A-C in the Supporting Information). Size distribution graph (Figure S2C in the Supporting Information) shows that some smaller particles appear, which are possibly attributed to the fragment from etched particles. To further understand the changes induced by NaOH etching, we performed nitrogen adsorption/desorption isotherms measurement (Figures S3 and S4 in the ESI†). Obvious hysteresis loop (Figure S3 in ESI†) indicates that mesopores are generated in m-SiO_2 NSs.[23] Since the solid SiO_2 NSs from stöber method are nonporous, the existence of the mesoporous morphology must be the result of NaOH etching. Pore size distribution (Figure S4 in ESI†) is rather narrow with a mean pore size of 11.13 nm. These pores provide enough spaces for CdTe QDs embedding into the silica network. TEM, HRTEM, and size distribution of CdTe QDs are shown in Figure S5 in ESI†. The diameter of CdTe QDs (2.64 nm) is smaller than the pores of m-SiO_2 NSs, thus CdTe QDs can facilely be embeded into the deep inside of mesopores without any steric hindrance. The HRTEM image (Figure S5B in ESI†) illustrates that CdTe QDs are well crystallized, and the lattice fringe with a spacing of about 0.34 nm is corresponding to the interplanar distance of the (200) plane in the cubic CdTe QDs.[24] From TEM and HRTEM in Figure 1C, it is found that CdTe QDs as small dots are well dispersed into m-SiO_2 matrix. The m-SiO_2/Ag NSs was also synthesized, and their TEM and HRTEM are given in Figure 1D. The Ag NPs with an average size of 28.32 nm (Figure S6 in ESI†) scatter sparsely on the surface of m-SiO_2 NSs. Interlayer spacing of 0.24 nm (the inset in Figure 1D) is assigned to the lattice spacing of (111) plane of Ag NPs.[25] On basis of HRTEM evident, we can prove that the surface attached nanoparticles are composed of Ag NPs. As shown in Figure 1E-H, the formation of m-SiO_2/CdTe/Ag NSs was confirmed by SEM, TEM, HRTEM, and EDX analysis. SEM and TEM images present that the as-prepared NSs are monodisperse and the surface immobilized Ag NPs have narrow size distribution (Figure 1E-G). Obviously, some relics

DOI: 10.1021/acsami.5b02472
ACS Appl. Mater. Interfaces 2015, 7, 10022−10033

with irregular morphology are visible in Figure 1F, which are possibly corresponding to the fragment from etched silica particles. Interlayer spacing of 0.34 and 0.24 nm in HRTEM (Figure 1G) implies that the NPs are composed of CdTe QDs and Ag NPs near the surface of m-SiO_2 NSs. The EDX pattern (Figure 1H) reveals the presence of CdTe and Ag along with m-SiO_2 NSs in the products. Elemental mappings (Figure 1I–P) illustrate the existence of different elements and the elemental distribution in the products, which further confirms the successful fabrication of m-SiO_2/CdTe/Ag NSs.

Figure 2A is the photos of m-SiO_2/CdTe/Ag NSs aqueous solution taken under the dark, visible, and UV lights. A red fluorescent color is observed by the naked eye, which suggests that m-SiO_2/CdTe/Ag NSs possess fluorescent properties. The crystalline of m-SiO_2/CdTe/Ag NSs was investigated by XRD analysis (Figure 2B). Three peaks at about 25, 41, and 47.0° correspond respectively to the (111), (220), and (311) planes, which are matched with the cubic zinc blende structure of CdTe crystal.[24] The peaks at around 59 and 65° assigned to the (400) and (331) planes of CdTe crystal are too weak to be detected. The XRD data also show diffraction peaks at about 38, 44, 65, and 78°, which could be assigned to the (111), (200), (220), and (311) planes of face-centered cubic Ag NPs.[25] The broad XRD reflection broad peak from 15 to 30° could be attributed to the diffraction of the amorphous structures of m-SiO_2 NSs.[26] The weakened peak intensities for CdTe QDs and Ag NPs can be explained by higher content of m-SiO_2 NSs in the products.[27] The presence of CdTe QDs and Ag NPs component were further verified by UV–visible absorption spectra (Figure 3C). The absorption peak maxima

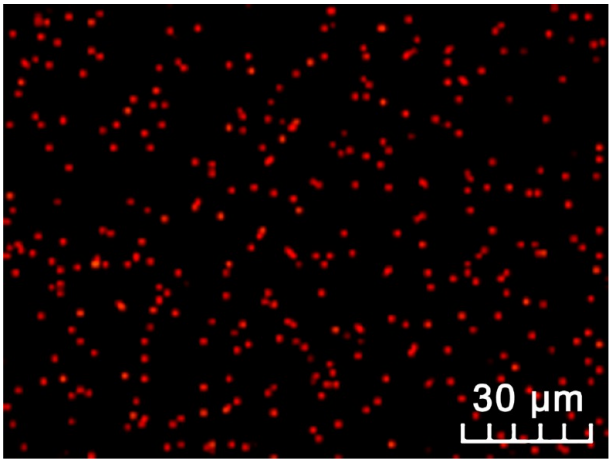

Figure 3. Fluorescence microscopy image (excitation λ = 365 nm) of m-SiO_2/CdTe/Ag NSs.

of 572 nm for CdTe QDs and 409 nm for Ag NPs are observed in UV–vis curve of m-SiO_2/CdTe/Ag NSs.[28,29] The m-SiO_2 NSs does not show any absorption at all within the whole range from 300 to 700 nm. FTIR spectra were applied to confirm the chemical binding of the products (Figure 2D). As for CdTe QDs, the stretching vibration of −COO-, S−H, and S−C are the most distinctive bands, which implies that the MPA binds firmly to CdTe QDs.[30] The strong peak at around 3500 cm^{-1} corresponds to the stretching vibration of −OH groups.[31] The intensities of these absorption peaks (−COO−, S−H, and S−C) are greatly weakened in the spectrum of m-SiO_2/CdTe NSs, which suggests that CdTe QDs are embedded into m-SiO_2 NSs. Besides, the peaks attributed to symmetric stretching vibration of Si−O−Si, stretching vibration of Si−O−H, and antisymmetric stretching vibration of Si−O−Si, acted as unique markers for silica component, are clearly detected in m-SiO_2/CdTe NSs.[32] Compared to m-SiO_2/CdTe NSs, a peak assigned to N−H stretching vibration from siliane coupling agent TSD attached to Ag NPs is noticed for m-SiO_2/CdTe/Ag NSs.[33] In Figure 3, the fluorescence microscopy images of m-SiO_2/CdTe/Ag NSs excited by a 365 nm UV beam show small red dots, which further confirm the loadings of CdTe QDs on the products.

The Ag NPs loading on m-SiO_2/CdTe NSs is key for this study, endowing the products with the attractive antibacterial properties. In this report, the loading of Ag NPs on the products is well controlled by tuning the $AgNO_3$/m-SiO_2/CdTe NSs mass/mass (M/M) ratio. The XRD pattern (Figure 4A) of m-SiO_2/CdTe/Ag NSs depicts that peaks for Ag NPs strengthen as the M/M ratio increases from 8.5/1 to 17/1, then to 34/1, suggesting that Ag NP content and M/M ratio show a good linear relationship. To explore the location and size of Ag NPs, we give SEM image and size distribution graphs of m-SiO_2/CdTe/Ag NSs prepared with different M/M ratios in Figure 4B-D. At lower M/M ratio of 8.5/1 (Figure 4B-1, C-1, and D-1), smaller Ag NPs with a higher loading are scattered uniformly all over the surface. Larger Ag NPs are observed as M/M ratio increases to 17/1 (Figure 4B-2, C-2, and D-2), but the loading amount of Ag NPs on the surface decreases and even some aggregation is detected. Further increasing the M/M ratio to 34/1 induces serious particle–particle aggregation, and only a few Ag NPs are sustained on the particle surface (Figure 4B-3, C-3, and D-3). As reported, the aggregated Ag NPs can release fewer Ag ions than the highly dispersed ones, so they always result in a loss of or a short time of antibacterial activity.[34] For another, compared to larger Ag NPs, the small Ag NPs have a faster release of Ag ions, thus displaying higher toxicity to bacteria. On the basis of a general consideration, m-SiO_2/CdTe/Ag NSs synthesized from lower M/M ratio of 8.5/1 is advantageous over the others.

To understand the effect of chemical bindings on fluorescent properties, we excited CdTe QDs, m-SiO_2/CdTe NSs, and m-SiO_2/CdTe/Ag NSs by UV light (λ = 365 nm) illumination, and their fluorescences were recorded comparatively. In Figure 5A, B, no significant reduction is observed in the fluorescence among them. The fluorescence spectrum (Figure 5B) shows a slight shift in the maximum emission wavelength from CdTe QDs, to m-SiO_2/CdTe NSs, then to m-SiO_2/CdTe/Ag NSs, which can be explained by the change in the ground-state and excited-state energies along with the change in the surrounding environments.[35] The fluorescence spectra of m-SiO_2/CdTe NSs and m-SiO_2/CdTe/Ag NSs before and after contacting bacteria are given in Figure 5C, D. As for m-SiO_2/CdTe NSs in Figure 5C, the fluorescence intensity shows drastic reduction after contacting bacteria, which confirms that CdTe QDs immobilized on the m-SiO_2 surface were easily attacked and consumed by bacteria.[36] Although a slight reduction is detected for fluorescence intensity of m-SiO_2/CdTe/Ag NSs when encountering bacteria. The most possible reason is that the outer Ag NPs can prevent bacteria invasion to avoid the direct contact between QDs with bacteria. Accordingly, we can conclude that immobilizing Ag NPs onto m-SiO_2/CdTe NSs can effectively protect CdTe QDs from bacteria invasion, thus giving excellent fluorescent property.

To understand the antibacterial capabilities, we performed the antibacterial test of m-SiO_2/CdTe NSs, m-SiO_2/Ag NSs,

DOI: 10.1021/acsami.5b02472
ACS Appl. Mater. Interfaces 2015, 7, 10022–10033

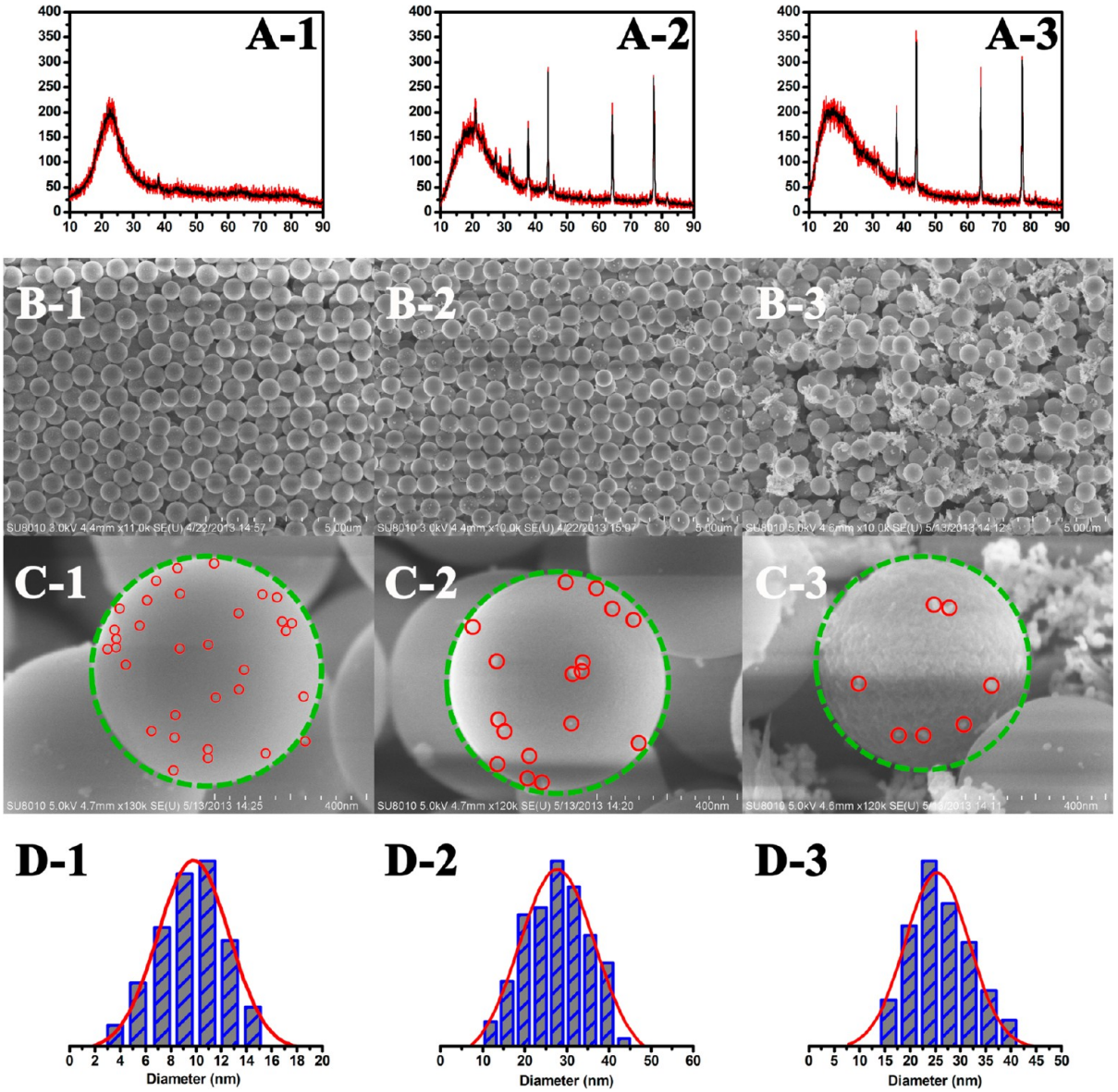

Figure 4. (A) XRD, (B, C) SEM, and (D) size distribution of m-SiO_2/CdTe/Ag NSs prepared with different $AgNO_3$/m-SiO_2/CdTe NSs mass/mass (M/M) ratio. A1−D1, 8.5/1; A2−D2, 17/1; A3−D3, 34/1.

and m-SiO_2/CdTe/Ag NSs using inhibition zone assay (Figure 6A). *S. aureus* and *E. coli* were selected as model bacteria. All three samples offer visible inhibition rings, suggesting that all they possess excellent antibacterial capabilities. Interestingly, the inhibition zone corresponding to m-SiO_2/CdTe NSs mirrors that CdTe QDs can inhibit bacteria growth by exhausting itself, which might be a suitable explanation for Figure 5C. Besides, we can also notice the differences in antibacterial activities among these three samples. As widely accepted, the value for inhibition ring represents the susceptibility of bacteria toward the antibiotics.[37] On the basis of this viewpoint, we can deduce that m-SiO_2/CdTe/Ag NSs is the most powerful, and m-SiO_2/CdTe NSs are the weakest. To further justify their differences in antibacterial activity, we quantitatively compared their antibacterial properties by measuring the viability of bacteria (Figure 6B). The bacterial suspension treated with the samples were spread onto LB-agar plates and incubated at 37 °C for 24 h. LB-agar plates containing no samples and m-SiO_2 NSs were used as comparative tests. The viability of colonies for both strains (*E. coli* and *S. aureus*) appears in LB-agar plates. The m-SiO_2/CdTe/Ag NSs completely kill colonies for both types of bacteria. Similar as the control group, m-SiO_2 NSs shows turbid plates, suggesting that m-SiO_2 NSs have no antibacterial function at all.[38] In contrast, both m-SiO_2/CdTe NSs and m-SiO_2/Ag NSs give decreased colony viability, showing visible bacteria-killing activity. Actually, the antibacterial power is in an order of m-SiO_2/CdTe/Ag > m-SiO_2/Ag > m-SiO_2/CdTe.

The Ag NPs are easily aggregated in media and resulted in a loss of antibacterial activity.[39] To evaluate the durability of m-SiO_2/CdTe/Ag NSs, we prolonged the incubation time from 24 h to 5 days, where there was still no *E. coli* colony (This results is the same as that in Figure 6B and not shown in Figures). For comparison, *E. coli* was also treated with the Ag NPs (the same silver concentration as m-SiO_2/CdTe/Ag NSs) with incubation time of 24 h and 5 days. As shown in Figure S7A, B in the Supporting Information, no viability is detected when incubating 24 h, whereas the 5 day incubated plate give

DOI: 10.1021/acsami.5b02472
ACS Appl. Mater. Interfaces 2015, 7, 10022−10033

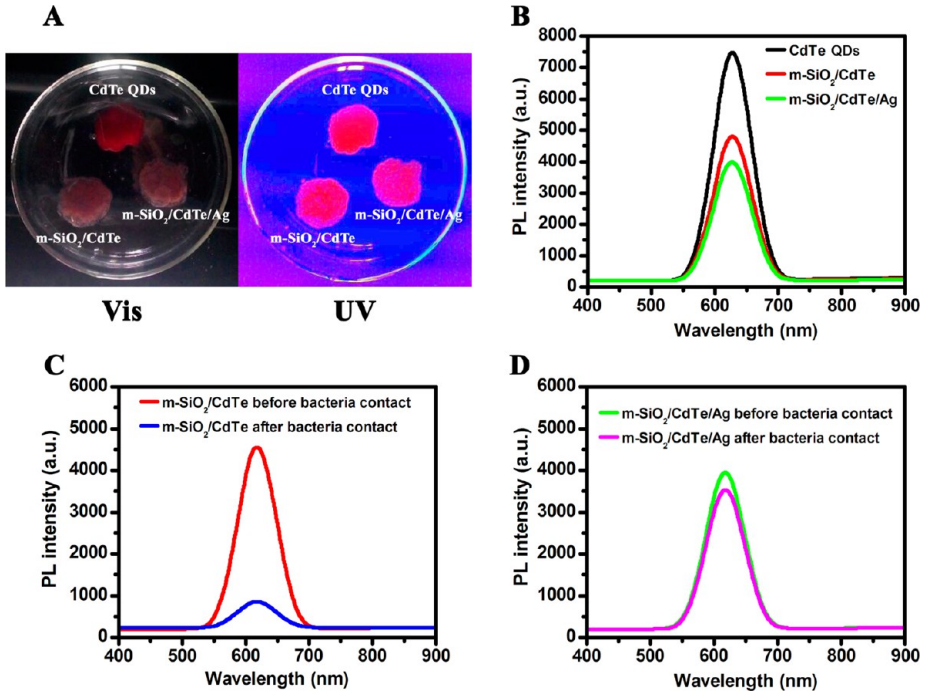

Figure 5. (A) Photos of CdTe QDs, m-SiO_2/CdTe NSs, and m-SiO_2/CdTe/Ag NSs under visible light and λ = 365 nm UV beam; (B) fluorescence emission spectrum of CdTe QDs, m-SiO_2/CdTe NSs, and m-SiO_2/CdTe/Ag NSs under λ = 365 nm UV beam; (C, D) fluorescence emission spectrum of (C) m-SiO_2/CdTe NSs and (D) m-SiO_2/CdTe/Ag NSs before and after bacteria contact under λ = 365 nm UV beam.

robust growth. It can be concluded that Ag NPs can only delay bacterial growth within a short time, but m-SiO_2/CdTe/Ag NSs possesses prolonged antibacterial property. We believe that m-SiO_2/CdTe/Ag NSs endow a long-term antibacterial activity because the supporting matrix m-SiO_2 can protect the Ag NPs from aggregation, and thus provide much more active sites on m-SiO_2 surfaces for killing bacteria. The Ag NPs without aggregation enable powerful and continuous antibacterial behaviors.

A time-kill assay was employed in our experiment to further clarify the antibacterial rate and extent of m-SiO_2/CdTe/Ag NSs. Figure 6C, D illustrates the time-kill graphs of m-SiO_2/CdTe/Ag NS suspension with different concentrations (from 0.1 to 5.0 mg/mL) toward *E. coli* and *S. aureus* as a function of contact time ranging from 0 to 360 min. For both two strains, the bacterial reduction shows faster rising speed first and then levels off with the aging time. Such a growing trend is in good agreement with those in the previous literatures.[40,41] The time-kill assay also shows a concentration-dependent manner of m-SiO_2/CdTe/Ag NSs against two strains. The antibiotic effects transform from inhibition to killing action when concentration increases.[42] The killing activity is fast-acting at the highest concentration of 5.0 mg/mL, and its end point is only 10 min for *E. coli* and 60 min for *S. aureus*, while the lowest concentration of 0.1 mg/mL gives end point of 240 min for *E. coli* and 360 min for *S. aureus*. It is evident that the concentration of m-SiO_2/CdTe/Ag NSs is the decisive factor for their antibiotic action.

The morphology of m-SiO_2/CdTe/Ag NSs after contacting *E. coli* for different times (10, 30, 60, 180, 240, and 360 min) was captured using TEM technique to explore morphological change (Figure 7A). The carriers m-SiO_2 NSs retain the original morphology without any differences among them. But the loading amount of Ag NPs on the surfaces obviously decreases with extending contact time. On closer observation, the decreasing trend in the sizes of Ag NPs is also found when contact time extends. The average diameter changes from 28.32 nm for 0 min to 12.27 nm for 360 min (Figure 7B). We speculate that the release action of Ag ions from m-SiO_2/CdTe/Ag NSs to solution during the antibacterial test is the most possible explanation for the morphology and size changes.

To further understand reason for the morphology and size changes, we established the developing trends of Cd and Ag content in m-SiO_2/CdTe/Ag NSs with increasing bacteria-contacting time using ICP analysis (Figure 7C). Before contacting bacteria, the Cd and Ag content in m-SiO_2/CdTe/Ag NSs is 3.73 and 4.21 wt %, respectively. It can be seen that in the region I Ag content decreases drastically when the contact time increase from 0 to 60 min. Interestingly, when extending aging time Ag content decreases gradually and even almost levels off finally in the region II. Such a tendency of Ag content is accordance with the changes in morphology and size in Figure 7A, B. The Cd content gives opposite mode, i.e., almost leveling off first (region I) and remarkable decrease subsequently (region II). Before 60 min, there is no obvious reduction found in Cd content, which suggests that CdTe QDs on m-SiO_2/CdTe/Ag NSs are not exhausted by contacting bacteria. Because Ag NPs with higher loading amount prevent the bacteria touching directly with CdTe QDs. When most of the Ag NPs are exhausted, Cd content decreases obviously after 60 min. On the basis of these data, we can conclude that CdTe QDs starts to loss as most of the Ag NPs is exhausted. In other words, the immobilization of Ag NPs onto m-SiO_2/CdTe NSs could prevent bacteria from invading CdTe QDs.

TEM and ICP analysis verify that Ag NPs are superior to CdTe QDs when they defend bacteria invasion. To explore the real cause, the zeta potentials of m-SiO_2 NSs, CdTe QDs, Ag NPs, *E. coli*, and *S. aureus* were analyzed as shown in Figure 7D and Figure S8 in the Supporting Information. Except for Ag NPs, all the others show negative potentials. The negative

DOI: 10.1021/acsami.5b02472
ACS Appl. Mater. Interfaces 2015, 7, 10022−10033

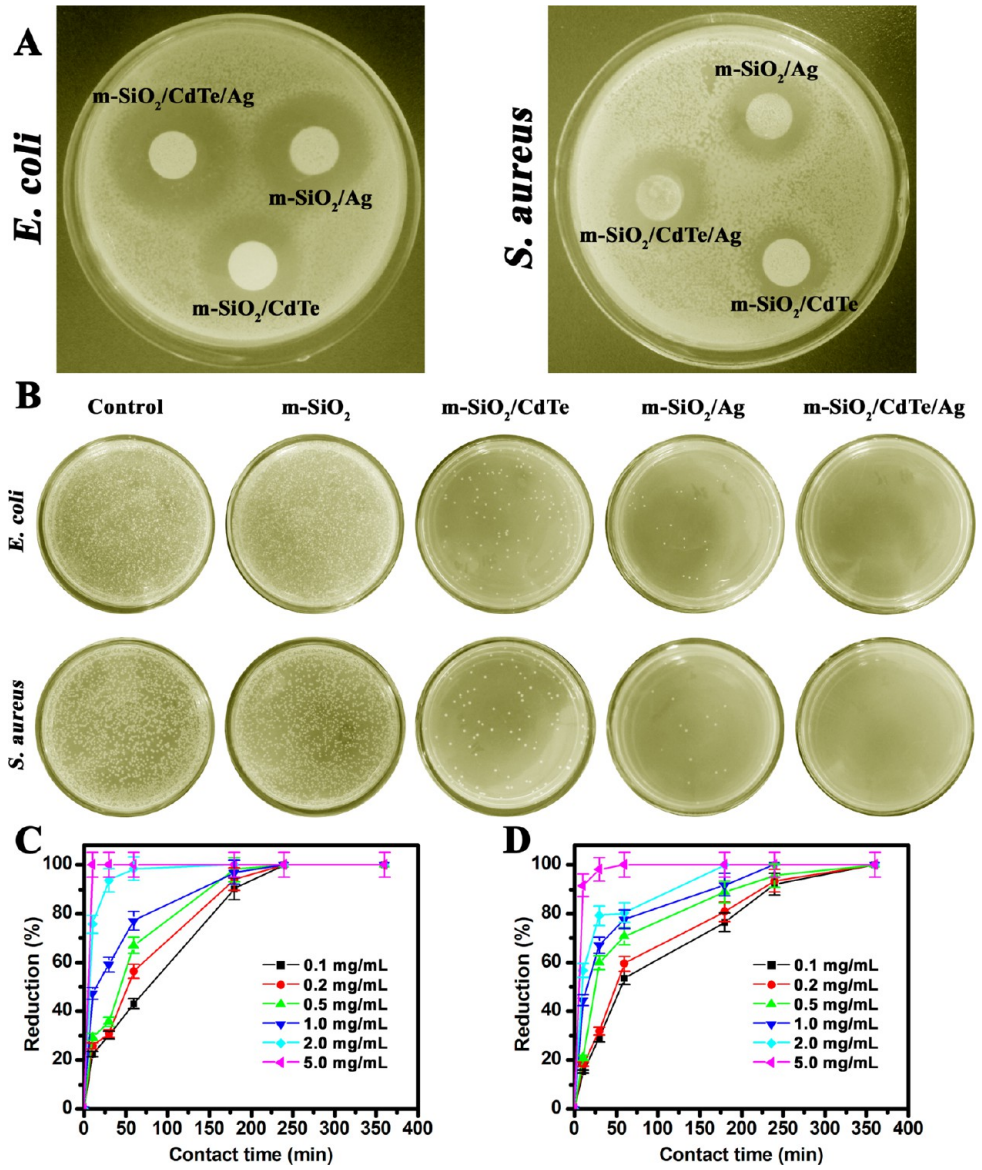

Figure 6. (A) Inhibition zone assay for m-SiO_2/Ag NSs, m-SiO_2/CdTe NSs, and m-SiO_2/CdTe/Ag NSs against *E. coli* and *S. aureus*; (B) photos showing the bacterial culture plates of *E. coli* and *S. aureus* upon 60 min exposure to 5 mg/mL m-SiO_2 NSs, m-SiO_2/CdTe NSs, m-SiO_2/Ag NSs, and m-SiO_2/CdTe/Ag NSs; (C, D) antibacterial time-kill assay graphs for m-SiO_2/CdTe/Ag NSs with different concentrations (0.1, 0.2, 0.5, 1.0, 2.0, and 5.0 mg/mL) against (C) *E. coli* and (D) *S. aureus* as a function of contact time. The bacterial reduction was calculated as the reduction % = $(B - A)/B \times 100\%$ (where A is the number of surviving bacterial colonies of the test sample and B is that of the control).

potentials of m-SiO_2 NSs and CdTe QDs are produced by the surface silanol groups and the carboxyl groups of the MPA, respectively. Indeed, both *E. coli* and *S. aureus* carry negative charges, and they can easily adhere to materials carrying positive charges, which were proven by previous works.[43] Smaller Ag NPs highly dispersed on the walls of m-SiO_2/CdTe NSs can release large amount of Ag ions, and thus they can exhibit positive potentials. Therefore, when the m-SiO_2/CdTe/Ag NS faces with bacteria, the positive charged Ag NPs combat first against bacteria, and in this way the CdTe QDs can be protected.

Our experiments demonstrate that m-SiO_2/CdTe/Ag NSs exhibit enhanced antibacterial activity toward both *E. coli* and *S. aureus*, which is closely related to the structure (well-dispersed Ag NPs), surface charge (positive zeta potentials), and size (small diameter) of Ag NPs. Previous studies summarized that the antibacterial mechanisms of Ag NPs can mainly be classified into two types including ion release mechanism and oxidation mechanism (Scheme 2).[44] As for m-SiO_2/CdTe/Ag NSs, it is possible that parts of Ag NPs on the surface of m-SiO_2/CdTe/Ag NSs are oxidized by dissolved oxygen to form Ag ions.[44] It is acceptable that Ag ions are easily accumulated around the living bacterial cells because of the special structure of bacteria and the negative charged bacterial surface.[44] The adsorbed Ag ions can interact with thiol group (−SH) of the cysteine chain by replacing the hydrogen atom to form S−Ag, which can hinder the enzymatic function of the protein to inhibit bacterial growth. Parts of Ag NPs can catalyze the dissolved oxygen to form reactive oxygen species, which have powerful oxidation capabilities.[44] On the basis of the plate counting method and inhibition zone test, we can speculate that the bacterial death induced by m-SiO_2/CdTe/Ag NSs is attributed to the integration the ion release mechanism with the oxidation mechanism for attacking bacteria.

DOI: 10.1021/acsami.5b02472
ACS Appl. Mater. Interfaces 2015, 7, 10022−10033

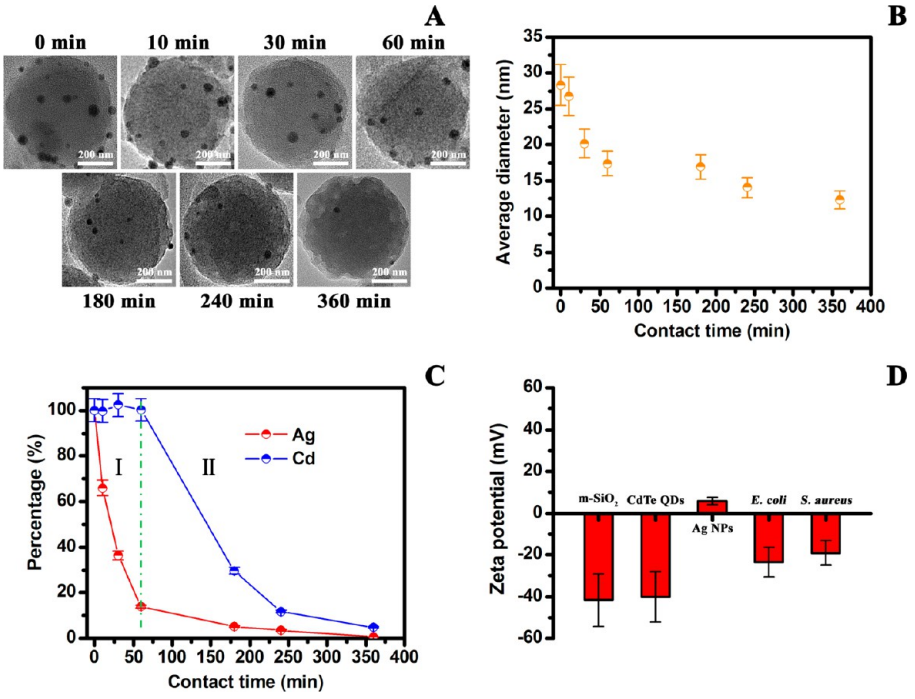

Figure 7. (A) TEM image of 0.1 mg/mL m-SiO_2/CdTe/Ag NSs, (B) the average diameter of Ag nanoparticles on m-SiO_2/CdTe/Ag NSs estimated by TEM, and (C) Ag and Cd content in m-SiO_2/CdTe/Ag NSs measured by ICP-MS after contacting 1×10^6 CFU/mL bacteria suspension for different contact time, respectively; (D) zeta potential of m-SiO_2 NSs, CdTe QDs, Ag NPs, *E. coli*, and *S. aureus*.

Scheme 2. Possible Antibacterial Mechanisms of m-SiO_2/CdTe/Ag NSs against Bacteria

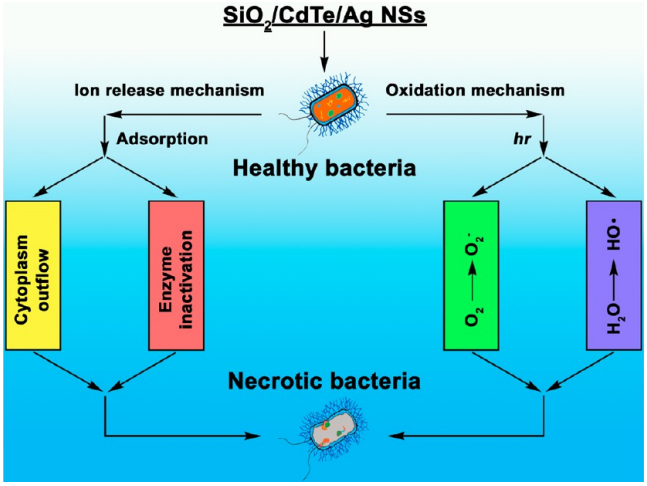

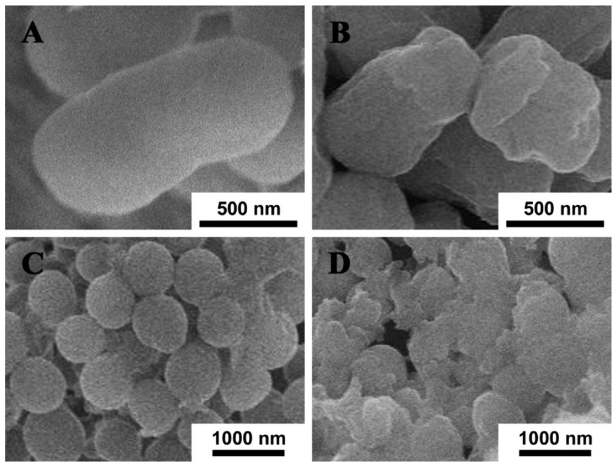

Figure 8. SEM images of (A, B) *E. coli* and(C, D) *S. aureus* (A, C) before and (B, D) after treating with 5.0 mg/mL of m-SiO_2/CdTe/Ag NSs for 360 min.

The SEM technique was employed to evaluate the morphological change in bacteria after treatment with m-SiO_2/CdTe/Ag NSs as shown in Figure 8. Live and dead bacteria were selected for morphological investigations to reveal the way of damaging. It is noted that the untreated *E. coli* and *S. aureus* have smooth and intact surfaces without cellular debris. Healthy *E. coli* is an obtuse corynebacteria with a smooth cell surface.[45] After contact with m-SiO_2/CdTe/Ag NSs, the rodlike shape of *E. coli* can no longer keep original integrity. The cell collapsed and corrugation is visible, giving a rugged surface. In comparison to intact *S. aureus* with a grapelike shape and smooth surface, morphology of the treated *S. aureus* significantly changes after the contact with m-SiO_2/CdTe/Ag NSs.[46] They present roughening and blebbing surface, and even some cell content of *S. aureus* is leaked. These results indicate that m-SiO_2/CdTe/Ag NSs can destroy bacterial surface structures.

The m-SiO_2/CdTe/Ag NSs integrated high fluorescent properties with powerful antibacterial activities can be applied in anticounterfeit applications such as security of tickets, certificates, money, checks, bank notes, trademarks, invoices, *etc*. To evaluate the potentials for the anticounterfeit applications, m-SiO_2/CdTe/Ag NSs were incorporated into a transparent ink to obtain UV light excited fluorescent anticounterfeit ink. Figure 9 shows the digital photographs of anticounterfeit labels painted in different modes with m-SiO_2/CdTe/Ag NSs ink under visible light and UV light irradiation. These paintings were clearly revealed under UV light (Figure 9-2), which is not quite obvious under visible light (Figure 9-1). To verify the long-term stability, we stored the paintings in a

DOI: 10.1021/acsami.5b02472
ACS Appl. Mater. Interfaces 2015, 7, 10022−10033

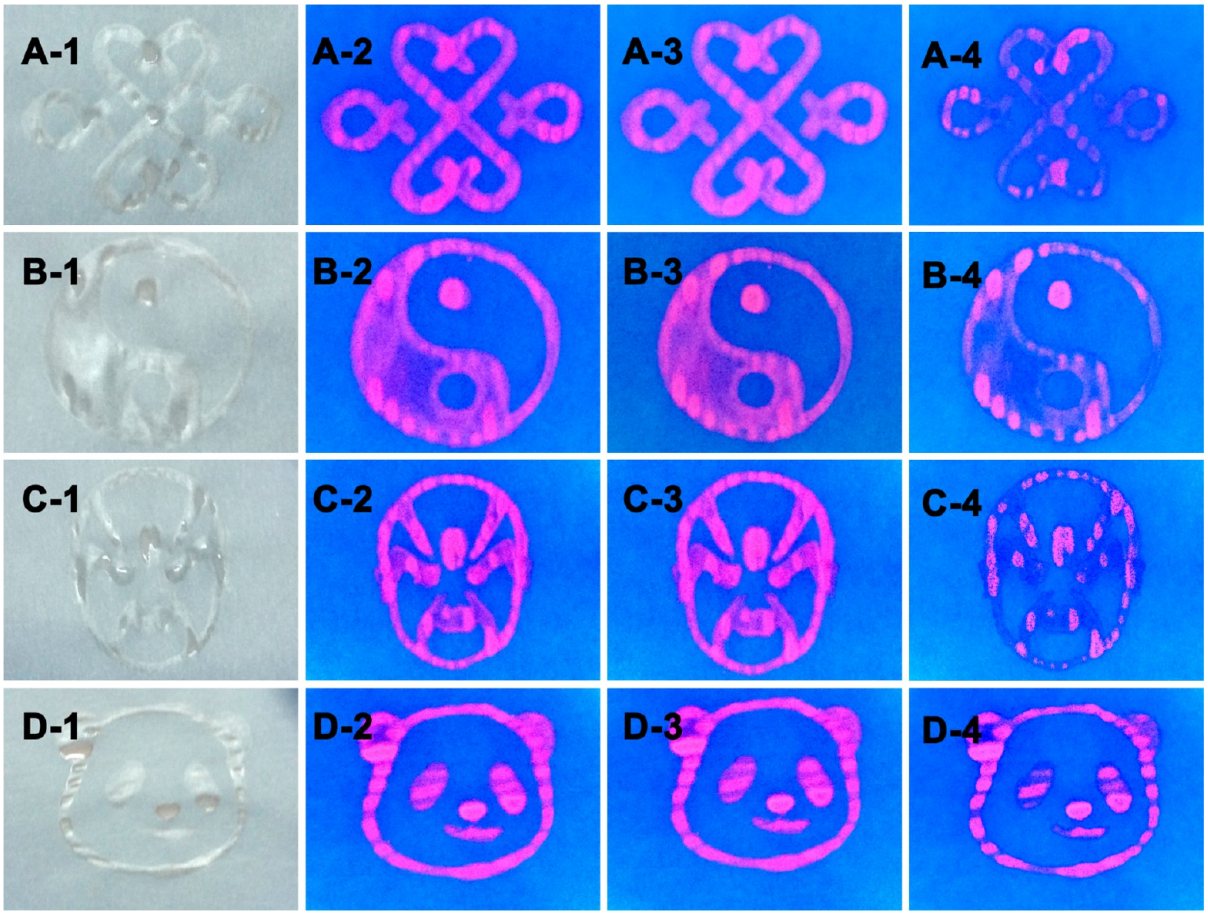

Figure 9. Anticounterfeit labels painted with m-SiO_2/CdTe/Ag NSs ink under (A1−D1) visible light and (A2−D2) UV light excitation. (A3−D3) Digital photographs of anticounterfeit labels after 6 months storage in 1 m^3 volume of *E. coli* dispersed casket under UV light excitation. (A4−D4) Digital photographs of anticounterfeit labels without Ag NPs component after storage in bacterial atmosphere for 6 months under UV light excitation.

1.0 m^3 closed system under bacterial atmosphere for six months. Notably from Figure 9-3, the fluorescent properties of m-SiO_2/CdTe/Ag NSs have been well preserved for more than six months without significant changes. For comparison, the paintings pretreated with "Ag NPs removal" procedure were also stored under bacterial atmosphere for 6 months. As expected, the paintings were seriously destroyed, which is obviously observed under UV irrigation (Figure 9-4). The experimental data further confirm the enhanced anticounterfeit applications of m-SiO_2/CdTe/Ag NSs.

CONCLUSIONS

In summary, fluorescent/antibacterial bifunctional nanomaterials, i.e., m-SiO_2/CdTe/Ag NSs, were skillfully designed and successfully synthesized by the aid of mesoporous silica carriers. Different techniques were applied to characterize m-SiO_2/CdTe/Ag NSs. Experiments prove that the loadings of Ag NPs on m-SiO_2/CdTe NSs are controllable, which is strongly related to their antibacterial capabilities. The CdTe QDs on m-SiO_2 NSs are vulnerable when encountering bacteria, whereas Ag NP-loaded m-SiO_2/CdTe/Ag NSs can protect CdTe QDs from bacterial invasion. The real reason for this fact is that the priority of Ag NPs over CdTe QDs to combat bacteria, which was explained by the zeta potentials. The most plausible antibacterial mechanisms of m-SiO_2/CdTe/Ag NSs were investigated. The possibility of using m-SiO_2/CdTe/Ag NS integrated excellent fluorescent properties and long-term antibacterial activities for potential in anticounterfeit applications was proven.

ASSOCIATED CONTENT

Supporting Information

Synthesis of solid SiO_2 NSs; synthesis of MPA modified CdTe QDs; synthesis of individually dispersed Ag NPs; SEM imgaes, TEM images, HRTEM image, and size distribution of solid SiO_2 NSs, m-SiO_2 NSs, CdTe QDs, and Ag NPs; nitrogen adsorption−desorption isotherm of solid SiO_2 NSs, m-SiO_2 NSs, m-SiO_2/CdTe NSs, and m-SiO_2/CdTe/Ag NSs; BJH pore-size distribution curves of solid SiO_2 NSs and m-SiO_2 NSs; Photographs showing the bacterial culture plates of *E. coli* treated with Ag NPs with incubation time of 24 h and 5 days; zeta potential of m-SiO_2 NSs (A), CdTe QDs (B), Ag NPs (C), *E. coli* (D), and *S. aureus* (E). The Supporting Information is available free of charge on the ACS Publications website at DOI: 10.1021/acsami.5b02472.

AUTHOR INFORMATION

Corresponding Author

*E-mail: dongali@imu.edu.cn. Tel.: +86 471 4992982.

Author Contributions

†Y.G. and Q.D. contributed equally to this work

DOI: 10.1021/acsami.5b02472
ACS Appl. Mater. Interfaces 2015, 7, 10022−10033

Notes

The authors declare no competing financial interest.

■ ACKNOWLEDGMENTS

This research was supported by the National Natural Science Foundation of China (21304044).

■ REFERENCES

(1) Han, G.; Mokari, T.; Ajo-Franklin, C.; Cohen, B. Caged Quantum Dots. *J. Am. Chem. Soc.* **2008**, *130*, 15811−15813.
(2) Wang, Y.; Hu, R.; Lin, G.; Roy, I.; Yong, K. Functionalized Quantum Dots for Biosensing and Bioimaging and Concerns on Toxicity. *ACS Appl. Mater. Interfaces* **2013**, *5*, 2786−2799.
(3) Li, Z.; Sun, Q.; Zhu, Y.; Tan, B.; Xu, Z. P.; Dou, S. X. Ultra-small Fluorescent Inorganic Nanoparticles for Bioimaging. *J. Mater. Chem. B* **2014**, *2*, 2793−2818.
(4) Wu, P.; Yan, X. Doped Quantum Dots for Chemo/Biosensing and Bioimaging. *Chem. Soc. Rev.* **2013**, *42*, 5489−5521.
(5) Zhang, Y.; Schnoes, A. M.; Clapp, A. R. Dithiocarbamates as Capping Ligands for Water-soluble Quantum Dots. *ACS Appl. Mater. Interfaces* **2010**, *2*, 3384−3395.
(6) Zhou, L.; Gao, C.; Hu, X.; Xu, W. One-Pot Large-Scale Synthesis of Robust Ultrafine Silica-Hybridized CdTe Quantum Dots. *ACS Appl. Mater. Interfaces* **2010**, *2*, 1211−1219.
(7) Xu, Z.; Deng, P.; Tang, S.; Kuang, D.; Zhang, F.; Li, J. Preparation of 2D Molecularly Imprinted Materials Based on Mesoporous Silica *via* Click Reaction. *J. Mater. Chem. B* **2014**, *2*, 8418−8426.
(8) Li, D.; He, X.; Chen, Y.; Li, W.; Zhang, Y. Novel Hybrid Structure Silica/CdTe/Molecularly Imprinted Polymer: Synthesis, Specific Recognition, and Quantitative Fluorescence Detection of Bovine Hemoglobin. *ACS Appl. Mater. Interfaces* **2013**, *5*, 12609−12616.
(9) Luo, Z.; Wu, Q.; Zhang, M.; Li, P.; Ding, Y. Cooperative Antimicrobial Activity of CdTe Quantum Dots with Rocephin and Fluorescence Monitoring for *Escherichia coli*. *J. Colloid Interface Sci.* **2011**, *362*, 100−106.
(10) Eckhardt, S.; Brunetto, P. S.; Gagnon, J.; Priebe, M.; Giese, B.; Fromm, K. M. Nanobio silver: Its Interactions with Peptides and Bacteria, and Its Uses in Medicine. *Chem. Rev.* **2013**, *113*, 4708−4754.
(11) Ocsoy, I.; Paret, M. L.; Ocsoy, M. A.; Kunwar, S.; Chen, T.; You, M.; Tan, W. Nanotechnology in Plant Disease Management: DNA-Directed Silver Nanoparticles on Graphene Oxide as an Antibacterial against *Xanthomonas perforans*. *ACS Nano* **2013**, *7*, 8972−8980.
(12) Cui, J.; Hu, C.; Yang, Y.; Wu, Y.; Yang, L.; Wang, Y.; Liu, Y.; Jiang, Z. Facile Fabrication of Carbonaceous Nanospheres Loaded with Silver Nanoparticles as Antibacterial Materials. *J. Mater. Chem.* **2012**, *22*, 8121−8126.
(13) Gao, N.; Chen, Y.; Jiang, J. Ag@Fe_2O_3-GO Nanocomposites Prepared by a Phase Transfer Method with Long-Term Antibacterial Property. *ACS Appl. Mater. Interfaces.* **2013**, *5*, 11307−11314.
(14) Zhang, L.; Luo, Q.; Zhang, F.; Zhang, D.; Wang, Y.; Sun, Y.; Dong, W.; Liu, J.; Huo, Q.; Sun, H. High-performance Magnetic Antimicrobial Janus Nanorods Decorated with Ag Nanoparticles. *J. Mater. Chem.* **2012**, *22*, 23741−23744.
(15) Zhang, L.; Dong, W.; Sun, H. Multifunctional Superparamagnetic Iron Oxide Nanoparticles: Design, Synthesis and Biomedical Photonic Applications. *Nanoscale* **2013**, *5*, 7664−7684.
(16) Li, C.; Jamison, A. C.; Rittikulsittichai, S.; Lee, T.; Lee, T. R. In Situ Growth of Hollow Gold-Silver Nanoshell within Porous Silica Offers Tunable Plasmonic Extinctions and Enhanced Colloidal Stability. *ACS Appl. Mater. Interfaces* **2014**, *6*, 19943−19950.
(17) He, D.; Ikeda-Ohno, A.; Boland, D. D.; Waite, T. D. Synthesis and Characterization of Antibacterial Silver Nanoparticle-Impregnated Rice Husks and Rice Husk Ash. *Environ. Sci. Technol.* **2013**, *47*, 5276−5284.
(18) Ma, J.; Zhang, J.; Xiong, Z.; Yong, Y.; Zhao, X. S. Preparation, Characterization and Antibacterial Properties of Silver-modified Graphene Oxide. *J. Mater. Chem.* **2011**, *21*, 3350−3352.
(19) Kumar, A. S.; Sornambikai, S.; Deepika, L.; Zen, J. Highly Selective Immobilization of Amoxicillin Antibiotic on Carbon Nanotube Modified Electrodes and Its Antibacterial Activity. *J. Mater. Chem.* **2010**, *20*, 10152−10158.
(20) Stöber, W.; Fink, A.; Bohn, E. Controlled Growth of Monodisperse Silica Spheres in the Micro Size Range. *J. Colloid Interface Sci.* **1968**, *26*, 62−69.
(21) Bai, W.; Nie, F.; Zheng, J.; Sheng, Q. Novel Silver Nanoparticles-Maganese Oxyhrdroxide-Graphene Oxide Nanocomposite Prepared by Modified Silver Mirror Reaction and Its Application for Electrochemical Sensing. *ACS Appl. Mater. Interfaces* **2014**, *6*, 5439−5449.
(22) Zhang, Q.; Zhang, T.; Ge, J.; Yin, Y. Permeable Silica Shell through Surface-Protected Etching. *Nano Lett.* **2008**, *8*, 2867−2871.
(23) Shin, H.; Hwang, Y.; Huh, S. Facile Preparation of Ultra-Large Pore Mesoporous Silica Nanoparticles and Their Application to the Encapsulation of Large Guest Molecules. *ACS Appl. Mater. Interfaces* **2014**, *6*, 1740−1746.
(24) Dong, W.; Cheng, Y.; Luo, L.; Li, X.; Wang, L.; Li, C.; Wang, L. Synthesis and Self-assembly of Hierarchical SiO_2-QDs@SiO_2 Nanostructures and Their Photoluminescence Applications for Fingerprint Detection and Cell Imaging. *RSC Adv.* **2014**, *4*, 45939−45945.
(25) Chen, K.; Pu, Y.; Chang, K.; Liang, Y.; Liu, C.; Yeh, J.; Shih, H.; Hsu, Y. Ag-Nanoparticle-Decorated SiO_2 Nanospheres Exhibiting Remarkable Plasmon-Mediated Photocatalytic Properties. *J. Phys. Chem. C* **2012**, *116*, 19039−19045.
(26) Dong, A.; Lan, S.; Huang, J.; Wang, T.; Zhao, T.; Wang, W.; Xiao, L.; Zheng, X.; Liu, F.; Gao, G.; Chen, Y. Preparation of Magnetically Separable *N*-Halamine Nanocomposites for the Improved Antibacterial Application. *J. Colloid Interface Sci.* **2011**, *364*, 333−340.
(27) Massey, M. S.; Lezama-Pacheco, J. S.; Nelson, J. M.; Fendorf, S.; Maher, K. Uranium incorporation into amorphous silica. *Environ. Sci. Technol.* **2014**, *48*, 8636−8644.
(28) Shan, Y.; Xu, J.; Chen, H. Enhanced Electrochemiluminescence Quenching of CdS: Mn Nanocrystals by CdTe QDs-Doped Silica Nanoparticles for Ultrasensitive Detection of Thrombin. *Nanoscale* **2011**, *3*, 2916−2923.
(29) Agnibotri, S.; Mukherji, S.; Mukherji, S. Immobilized Silver Nanoparticles Enhance Contact Killing and Show Highest Efficacy: Elucidation of the Mechanism of Bactericidal Action of Silver. *Nanoscale* **2013**, *5*, 7328−7340.
(30) Liang, Q.; Ma, W.; Shi, Y.; Li, Z.; Yang, X. Easy Synthesis of Highly Fluorescent Carbon Quantum Dots from Gelatin and Their Luminescent Properties and Applications. *Carbon* **2013**, *60*, 421−428.
(31) Song, J.; Kang, H.; Lee, C.; Hwang, S. H.; Jang, J. Aqueous Synthesis of Silver Nanoparticle Embedded Cationic Polymer Nanofibers and Their Antibacterial Activity. *ACS Appl. Mater. Interfaces* **2012**, *4*, 460−465.
(32) Dong, A.; Lan, S.; Huang, J.; Wang, T.; Zhao, T.; Xiao, L.; Wang, W.; Zheng, X.; Liu, F.; Gao, G.; Chen, Y. Modifing Fe_3O_4-Functionalized Nanoparticles with *N*-Halamine and Their Magnetic/Antibacterial Properties. *ACS Appl. Mater. Interfaces* **2011**, *3*, 4228−4235.
(33) Dong, A.; Huang, J.; Lan, S.; Wang, T.; Xiao, L.; Wang, W.; Zhao, T.; Zheng, X.; Liu, F.; Gao, G.; Chen, Y. Synthesis of *N*-Halamine-Functionalized Silica-Polymer Core-Shell Nanoparticles and Their Enhanced Antibacterial Activity. *Nanotechnology* **2011**, *22*, 295602.
(34) Sotiriou, G.; Meyer, A.; Knijnenburg, J. T. N.; Panke, S.; Pratsinis, S. Quantifying the Origin of Released Ag^+ Ions from Nanosilver. *Langmuir* **2012**, *28*, 15929−15936.
(35) Zhang, Q.; Dong, A.; Zhai, Y.; Liu, F.; Gao, G. Synthesis of 1,4-Bis(*o*-cyanostyryl)benzene-Silica Nanoparticles with Core-Shell Structures and Effects of Reaction Conditions. *J. Phys. Chem. C* **2009**, *113*, 12033−12039.

DOI: 10.1021/acsami.5b02472
ACS Appl. Mater. Interfaces 2015, 7, 10022−10033

(36) Kumar, H.; Srivastava, R.; Dutta, P. K. Highly Luminescent Chitosan-L-cysteine Functionalized CdTe Quantum Dots Film: Synthesis and Characterization. *Carbohydr. Polym.* **2013**, *97*, 327−334.
(37) Dong, A.; Sun, Y.; Wang, Q.; Cai, Q.; Qi, X.; Zhang, Y.; Gao, G.; Liu, F.; Harnoode, C. Barbituric acid-based Magnetic *N*-Halamine Nanoparticles as Recyclable Antibacterial Agents. *ACS Appl. Mater. Interfaces* **2013**, *5*, 8125−8133.
(38) Li, C.; Hou, J.; Huang, Z.; Zhao, T.; Xiao, L.; Gao, G.; Harnoode, C.; Dong, A. Assessment of 2,2,6,6-Tetramethly-4-piperidinol-based Amine *N*-Halamine-labeled Silica Nanoparticles as Potent Antibiotics for Deactivating Bacteria. *Colloids Surf., B* **2015**, *126*, 106−114.
(39) Boomi, P.; Prabu, H. G.; Mathiyarasu, J. Synthesis and Characterization of Polyaniline/Ag-Pt Nanocomposite for Improved Antibacterial Activity. *Colloids Surf., B* **2013**, *103*, 9−14.
(40) Kong, H.; Song, J.; Jang, J. One-step Fabrication of Magnetic γ-Fe_2O_3/Polyrhodanine Nanoparticles Using in Situ Chemical Oxidation Polymerization and Their Antibacterial Properties. *Chem. Commun.* **2010**, *46*, 6735−6737.
(41) Li, C.; Xue, L.; Cai, Q.; Bao, S.; Zhao, T.; Xiao, L.; Gao, G.; Harnoode, C.; Dong, A. Design, Synthesis and Biocidal Effect of Novel Amine *N*-Halamine Microshperes Based on 2,2,6,6-Tetramethyl-4-piperidinol as Promising Antibacterial Agents. *RSC Adv.* **2014**, *4*, 47853−47864.
(42) Zhang, X.; Chibli, H.; Mielke, R.; Nadeau, J. Ultrasmall Gold-Doxorubicin Conjugates Rapidly Kill Apoptosis-Resistant Cancer Cells. *Bioconjugate Chem.* **2011**, *22*, 235−243.
(43) Tian, Y.; Qi, J.; Zhang, W.; Cai, Q.; Jiang, X. Facile, One-pot Synthesis, and Antibacterial Activity of Mesoporous Silica Nanoparticles Decorated with Well-dispersed Silver Nanoparticles. *ACS Appl. Mater. Interfaces* **2014**, *6*, 12038−12045.
(44) Wang, X.; Dai, Y.; Zou, J.; Meng, L.; Ishikawa, S.; Li, S.; Abuobeidah, M.; Fu, H. Characteristics and Antibacterial Activity of Ag-embedded Fe_3O_4@SiO_2 Magnetic Composite as a Reusable Water Disinfectant. *RSC Adv.* **2013**, *3*, 11751−11758.
(45) Flemke, J.; Maywald, M.; Sieber, V. Encapsulation of Living *E. coli* Cells in Hollow Polymer Microspheres of Highly Defined Size. *Biomacromolecules* **2013**, *14*, 207−214.
(46) Hsu, S.; Tseng, H.; Hung, H.; Wang, M.; Hung, C.; Li, P.; Lin, J. Antimicrobial Activities and Cellular Responses to Natural Silicate Clays and Derivatives Modified by Cationic Alkylamine Salts. *ACS Appl. Mater. Interfaces* **2009**, *1*, 2556−2564.

DOI: 10.1021/acsami.5b02472
ACS Appl. Mater. Interfaces 2015, 7, 10022−10033